Internal strain and dynamic effective charges in CuCl and CuBr

M. R. Press and D. E. Ellis
Materials Research Center and Department of Physics and Astronomy, Northwestern University, Evanston, Illinois 60201
(Received 23 December 1987)

Self-consistent local-density theory has been used in the embedded-molecular-cluster framework to study the internal strain and response of the electronic charge distribution to external fields in CuCl and CuBr. The piezoelectric response and dynamic effective charges have been determined following the formalism developed by Martin. We find that rather small clusters are able to reproduce energy-level features deduced from experiment and band-structure models. The bulk lattice constant is reproduced to within 4% and calculated deformation properties show that the Cu–halogen bond is relatively rigid.

I. INTRODUCTION

The tetrahedrally coordinated halides of Cu and Ag are isomorphic with the diamondlike semiconductors. The isolated metal and halogen atoms have nominally $d^{10}s^1$ and s^2p^5 outer electronic configurations: in the compound, the loosely bound s electron of the metal is mostly transferred to the more electronegative halogen. Now the completely filled outer d shell of the noble metal is not corelike as in the valence metal levels of alkali halides; the spatial extent of the d levels is large, they reside near the Fermi energy, and they are close to the halogen p levels so that their hybridization significantly influences the chemical behavior of these compounds. Consequently, over the course of the last decade, the halides of copper, namely CuCl, CuBr, and CuI have acquired a wealth of intriguing literature, primarily because they refuse to follow well-defined trends in electroelastic properties and due to the peculiarities in their physical properties and phonon dispersion relations. They crystallize in the zinc-blende structure and are among the most ionic of the AB-type compounds that have tetrahedral covalent structure; their Phillips ionicity values[1] range from 0.746 for CuCl to 0.735 for CuBr to 0.692 for CuI. In Martin's parametrized model[2] of the elastic and piezoelectric properties in zinc-blende and wurtzite structures, these halides exhibit a striking decrease in the elastic-constant invariants such as the reduced bulk moduli and the reduced shear constants: for instance, their bulk moduli are only $\frac{1}{5}$ of the values typical of II-VI semiconductors. This is in agreement with the basic idea of the Phillips theory, that crystals with an ionicity greater than 0.785 occur in the rocksalt or CsCl structure. Thus, the Cu halides seem to approach an elastic instability as the critical ionicity is reached. Hanson *et al.*[3] have measured the piezoelectric constant of CuCl, $e_{14}=0.34$ C/m^2, to be the largest among the entire group of zinc-blende and wurtzite semiconductors; CuBr and CuI are not far behind at $e_{14}=0.27$ and 0.13 C/m^2. Other observations of anomalous properties of CuCl (Ref. 4) include a breakdown of the Lyddane-Sachs-Teller relation at ambient pressure, a 10^6 change in resistivity at moderately high pressure, an unusually large diamagnetic susceptibility anomaly above 90 K in rapidly cooled samples, superionic behavior, irregular value of the thermal expansion coefficient with temperature, and a number of structural transitions with pressure.

With the recent advances in thin-film technology, Wong *et al.*[5] have succeeded in fabricating a novel semiconductor compositionally modulated structure (CMS), CuCl/CuBr, grown along the [111] direction. The lattice mismatch between the two constituents is small enough (5.3%) to be accommodated by a coherency strain, which when coupled with the difference in piezoelectric constants causes the CMS to exhibit a net measurable permanent ferroelectric moment. Further, the wavelength modulation in composition produces new Bragg planes which result in additional optic modes corresponding to acoustic and optic phonons folded back to the zone center by the CMS periodicity; these modes can be coherently driven by the electric field of a far-infrared light wave, thereby making possible the generation of tunable coherent high-frequency phonons in piezoelectric transducers. The present study was motivated by these experimental developments. However, before proceeding to the understanding of the physics in this CMS, one requires an adequate characterization of the host materials themselves. In the present work we have focused on (a) structural properties—lattice constant, cohesive energies and bulk moduli, (b) self-consistent determination of internal strains, and (c) electrooptic parameters that embody the response of a piezoelectric to local and macroscopic electric fields under applied stresses, e.g., the transverse (or Born) effective charge e_T, the quadrupolar induced charge density Q, and the piezoelectric constant e_{14}.

II. THE PIEZOELECTRIC FORMULATION

The piezoelectric effect[6] refers to the production of the electric polarization by application of stress to a crystal. The change in polarization $\mathbf{P}$ produced to lowest order when a strain $S_{\beta\gamma}$ is applied is given by

$$P_\alpha=\sum_{\beta,\gamma} e_{\alpha\beta\gamma}S_{\beta\gamma}+\sum_{\beta}\chi_{\alpha\beta}E_\beta\ . \tag{1}$$

Here, α, β, and γ are Cartesian coordinates, and $\mathbf{E}$ is the macroscopic electric field. The piezoelectric constant $e_{\alpha\beta\gamma}$ is the polarization produced per unit strain at constant $\mathbf{E}$, and $\chi_{\alpha\beta}=(1/4\pi)(\epsilon_{\alpha\beta}-1)$ is the dielectric susceptibility. In the long-wavelength limit of a phonon mode of wave vector $\mathbf{k}$ propagating through an infinite crystal, Martin[2,7] has shown that the polarization can be expressed in terms of the dipole and quadrupole moments of the charge density induced by displacement of individual atoms

$$P_\alpha=\frac{1}{V_0}(Q_{\alpha\beta\gamma}S_{\beta\gamma}+e^*_{K\alpha\beta}u_{K\beta})+\chi_{\alpha\beta}E_\beta \ . \tag{2}$$

The derivation of the expressions for e^* and Q proceeds as follows. Let the induced charge density caused by displacement of the atom at $\mathbf{R}_{lK}$ in cell l be

$$F_{K\alpha}(\mathbf{r}-\mathbf{R}_{lK})=\frac{\partial\rho(\mathbf{r})}{\partial\mathbf{R}_{lK\alpha}} \ . \tag{3}$$

Then the total induced charge density $\delta\rho$ is the sum of all the contributions caused by the displacements of each atom

$$\delta\rho(\mathbf{r})=\sum_{l,K,\alpha}\left.\frac{\partial\rho(\mathbf{r})}{\partial R_{lK\alpha}}\right|_{\mathbf{R},\mathbf{E}} u_{lK\alpha} \ , \tag{4}$$

where $u_{lK\alpha}$ is the displacement of the atom at $\mathbf{R}_{lK}$. From $\nabla\cdot\mathbf{P}=-4\pi\delta\rho(\mathbf{r})$, the kth Fourier component of the polarization is given by

$$-i\mathbf{k}\cdot\mathbf{P}=\frac{1}{V}\sum_{K,\alpha}\int d^3r\, e^{-i\mathbf{k}\cdot\mathbf{r}}F_{K\alpha}(\mathbf{r}-\mathbf{R}_{lK})u_{lK\alpha} \ . \tag{5}$$

In the long-wavelength limit of an optic mode for which $u_{lK\alpha}=u_{K\alpha}\exp(i\mathbf{k}\cdot\mathbf{R}_{lK\alpha})$, the average over the entire crystal in Eq. (5) is independent of cell m and can be written to lowest order in $\mathbf{k}$ as

$$\hat{\mathbf{k}}\cdot\mathbf{P}=\frac{1}{V_0}\sum_\alpha\int d\mathbf{r}(\hat{\mathbf{k}}\cdot\mathbf{r})F_{K\alpha}(\mathbf{r})u_{K\alpha} \ , \tag{6}$$

where V_0 is the volume of a unit cell. By comparison with Eq. (2),

$$e^*_{K\alpha\beta}=\int d^3r\, r_\alpha F_{K\beta}(\mathbf{r}) \tag{7}$$

is the effective charge for atoms of species K, and satisfies the neutrality condition $\sum_K e^*_K=0$. Also,

$$Q_{\alpha\beta\gamma}=\int d^3r\, r_\alpha\sum_K F_{K\beta}(\mathbf{r})r_\gamma \tag{8}$$

is the quadrupole moment tensor of the induced charge density.

It is essential here to differentiate between cases when the polarization $\mathbf{P}$ is perpendicular to $\mathbf{k}$ and when it is parallel to $\mathbf{k}$. In the transverse geometry $\mathbf{k}\perp\mathbf{P}$, the macroscopic electric field vanishes. In the longitudinal geometry, $\mathbf{k}\parallel\mathbf{P}$, $\mathbf{E}=-4\pi\mathbf{P}$, so that $\mathbf{E}$ can be eliminated from Eq. (1) giving

$$(\mathbf{P}_L)_\alpha=\frac{1}{V_0}\frac{1}{\epsilon_{\alpha\delta}}(Q_{\delta\beta\gamma}e_{\beta\gamma}+e^*_{K\delta\beta}u_{K\beta}) \ . \tag{9}$$

Then the longitudinal and transverse coefficients are related by

$$(e^*_L)_{K\alpha\beta}=\frac{1}{\epsilon_{\alpha\gamma}}e^*_{K\delta\beta} \ , \tag{10a}$$

$$(Q_L)_{\alpha\beta\gamma}=\frac{1}{\epsilon_{\alpha\delta}}Q_{\delta\beta\gamma} \ . \tag{10b}$$

Several comments are in order regarding the above formulation. In both geometries, the integrals in Eqs. (7) and (8) are convergent and uniquely defined. The results hold also for a uniform unsymmetrized strain in a finite crystal. A purely macroscopic strain S generates a piezoelectric polarization only through the quadrupole moment Q [see Eq. (2)] since the dipole moments of different atoms K cancel identically. Since in general a strain is accompanied by internal optic displacements u which can be determined by minimizing the total energy, Q is only a part of the piezoelectric constant. The transverse effective charge is the exact coefficient of the internal-strain term. We have thus identified the contributions to the piezoelectric constant from (a) the motion of the ions and (b) the delocalization of charge amongst positive and negative ions when the crystal is strained.

A convenient method of obtaining e^* and Q is to calculate[8] the self-consistent charge density of the crystal with just one lattice plane of atoms, say $P(z=0)$, displaced in a widely spaced manner so that we can write e^*_L and Q_L in terms of well-defined integrals over the two-dimensional function

$$H_{K\beta}(\mathbf{r})=\sum_m F_{K\beta}(\mathbf{r}-\mathbf{R}_{mK}) \ ,$$

i.e.,

$$(e^*_L)_{K\beta}=\int dz\, z\int d^2r\, H_{K\beta}(z) \tag{11a}$$

and

$$\hat{K}_\alpha(Q_L)_{\alpha\beta\gamma}\hat{K}_\gamma=\sum_K\int dz\, z^2\int d^2r\, H_{K\beta}(z) \ . \tag{11b}$$

In zinc-blende structure, a purely longitudinal piezoelectric effect appears for uniaxial strain ϵ along the [111] direction, $P=(2/\sqrt{3})e_{14}\epsilon$.[9] The sublattice displacement is now a linear function of the macroscopic strain ϵ and, following Kleinman,[10] is given by the conventional dimensionless internal strain parameter ζ. With z as the coordinate along the [111] direction, the piezoelectric constant can be written as

$$e_{14}=\frac{1}{8}\frac{\zeta_a}{V_0}\int d^3r\, z[f_{1z}(\mathbf{r})-f_{2z}(\mathbf{r})] -\frac{\sqrt{3}}{4}\frac{1}{V_0}\int d^3r\, z^2[f_{1z}(\mathbf{r})+f_{2z}(\mathbf{r})] \tag{12a}$$

or more compactly in dimensionless form as

$$\frac{a^2}{e}e_{14}=\zeta(e^*_T/e)-\Delta Q \ . \tag{12b}$$

III. METHODOLOGY

The LCAO-MO method for embedded molecular clusters within the framework of the Hartree-Fock-Slater

local-density formalism used in this work has been described in detail in the literature.[11] The successes and limitations of extracting the cohesive energy within this framework for several simple solids have also been explored in a recent thesis[12] and in studies on NaCl-structure oxides.[13] We shall thus limit our discussion here to the specific aspects of the present calculation. Our particular interest in the geometry along the [111] direction has led to the choice of two unusually shaped basic clusters. A neutral 14-atom ellipsoidal-shaped cluster, $Cl_1Cu_3Cl_3Cu_3Cl_3Cu$, has no central region and no cluster atom whose fourfold tetrahedral coordination is complete within the cluster. A neutral eight-atom cluster $Cl_3CuClCu_3$ [see Fig. 1(b)] has one Cu atom and one halide atom with full tetrahedral coordination within the cluster. Each cluster has C_{3v} symmetry about the principal $\hat{\mathbf{z}}\|[111]$ axis; atom species placed at different z values constitute inequivalent sets. Since the layer-pair stacking sequence is 012012... along [111], the repeating cell is conveniently chosen to consist of one atom in each of the three-layer pairs. The microcrystal, i.e., the set of crystal atoms around the cluster providing a self-consistent crystal field in which the cluster is embedded, is correspondingly molded to the shape of the variational cluster; it is cylindrically shaped along the [111] axis and depending on the lattice parameter consists of between 200 and 225 of the nearest Cu and halide atoms. Experience has shown that a near-minimal atomic basis set, consisting of say three variational orbitals per atom (e.g., $3d,4s,4p$ for Cu and ns,np,nd for the halide), is adequate for charge-density analysis and for obtaining the density of states. For calculating the total energy and for extracting the cohesive energy, a more complete basis set is selected in which to expand the crystal charge density and crystal potential: $3s^23p^63d^{10}4s^14p^05s^05p^0$ for Cu, $3s^23p^53d^04s^04p^0$ for Cl, and $4s^24p^54d^05s^05p^0$ for Br. To control lattice-sum convergence while maintaining variational flexibility in a solid, the tails of the extended orbitals are severely compressed by means of a potential well of depth 3.0 a.u. extending out to a radius of 4.0 a.u. and truncated sharply at 6.0 a.u. For each atom the lower-lying orbitals constitute the nonvariational or "frozen" core. The legitimacy of this step comes from the assertion that the shift in energy of the deepest-lying core orbitals that do not participate in the self-consistency procedure is given to satisfactory precision by the first-order approximation $\int \rho_0^c(\mathbf{r})\Delta V(\mathbf{r})d\mathbf{r}$, and numerous tests on molecular systems.

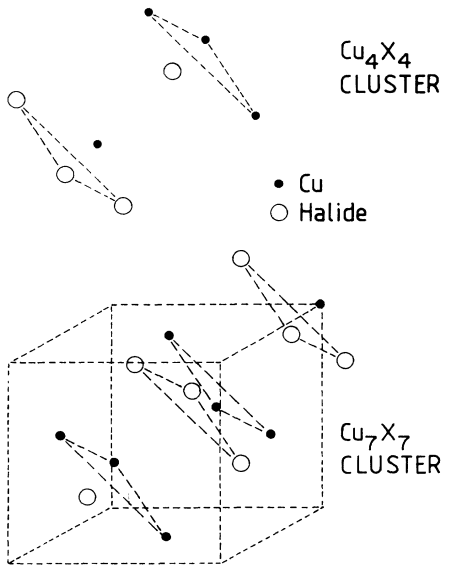

FIG. 1. The basic clusters. X denotes the halide atom in the chemical formulas Cu_4X_4, Cu_7X_7.

The self-consistent potential and the charge density are averaged over the different Cu atoms and the different halide atoms separately in the cluster in order to minimize size effects. The coefficients in the charge density expansion are determined by a least-squares fit to the exact cluster charge density obtained from the occupied wave functions that are solutions to the system Hamiltonian. These coefficients are then attributed also to the appropriate atoms in the microcrystal external to the cluster; thus the crystal potential generated varies from cycle to self-consistent cycle so as to match the potential from the cluster atoms. When coupled together, these two steps ensure a perfectly periodic crystalline solid.

The electrostatic crystal potential and the electrostatic energy are evaluated using a combination of real-space and Fourier-space computations, by a generalized Ewald summation, such that the largest term neglected in the Coulomb potential summation is of the order of 3×10^{-10} a.u. The value of the parameter α in the HFS-$X\alpha$ approximation to the local exchange potential is maintained constant at $\alpha=0.70$ in all our calculations. About 600 sampling points per cluster cation and 650 points per cluster anion are distributed between a Gauss-quadrature grid around the nucleus of 12 angular points at each of 40 radial steps out to 1.5 a.u. and a quasirandom diophantine set of points in the interstitial region. The cohesive energy is converged to only $\sim$0.75 eV with respect to this particular sampling operator density; we estimate that an increase to about 1200 points per atom is required to converge to cohesive energy to within 0.04 eV. This would be a computationally heavy step, rendered moot by the fact that the absolute position of the cohesion curve on the energy axis is equally sensitive to the values of other model parameters discussed below. Fortunately, the quantities of interest depend essentially upon *differences* in energy and charge density, which are not very sensitive. The cohesive energies per formula unit have been calculated using various volumes of integration corresponding to a primitive cell with one Cu–halide-ion pair or a proper unit cell with four Cu-halide pairs or a repeating cell along the [111] direction with parameter $c=\sqrt{3}a$. These different integration volumes give identical results, lending confidence to our numerical procedures. Indeed once the self-consistent charge densities and cluster eigenvalue spectra have been obtained in the fully periodic solid, we are at liberty to employ clusters of any shape and size to compute the discrete-volume-integral terms in the expression for the total and cohesive energy.

IV. RESULTS

A. Structural properties

We first present the cohesive energy versus lattice volume parameter calculations. The cohesive energy was evaluated for 5–7 values of the lattice constant and the points closest to the minimum were fitted to a second-order polynomial from which the equilibrium properties of the solid are derived. The calculated values for the equilibrium lattice constant, cohesive energy and the bulk modulus are presented in Table I. These calculations are performed with the halide sublattice at the ideal position $\frac{1}{4}$ way along the body diagonal: we shall see later that the shape and size of the cluster chosen strongly influences the equilibrium position of the sublattice and must be accounted for before deformation properties of the crystal can be extracted.

First it is important to note the discernible dispersion of the calculated energy values about the fit in Figs. 2(a) and 2(b). The explanation for this lies in the values of the self-consistent occupation numbers that result for the "unoccupied" excited-state diffuse orbitals of Cu, Cl, and Br. In Table II, we have summarized the features of the charge-density analysis and the derived density of states (DOS). The least-squares-fitting procedure gives sizeable occupations (both positive and negative) of $4p, 5s, 5p$ for Cu, $3d, 4s, 4p$ for Cl in CuCl, and $4d, 5s, 5p$ for Br. This is an outcome of a purely mathematical unconstrained fitting procedure minimizing the mean-square error. The only really relevant quantity is the sum charge carried by all the diffuse orbitals, e.g., $q(4p+5s+5p)=0.44$ for Cu and $q(3d+4s+4p)=0.413$ for Cl in CuCl, which are reasonable numbers. The charge density corresponding to these amplitudes resides well away from the nucleus and the atom-centered sampling-point generator is better geared towards the core and valence regions. So as the lattice parameter is varied, changes in these amplitudes are an order of magnitude greater than the changes in the occupations of the nominally occupied orbitals and it is that much more difficult to attain their convergence. More importantly, this also implies that the Coulomb potential and the charge density do not have the same r-space cutoff; even then any reasonable radius at which such an extended charge density is terminated will be the source of large truncation errors in the $\rho^{1/3}$ functional form of the exchange-correlation potential. The too large value of the bulk moduli we obtain for these compounds

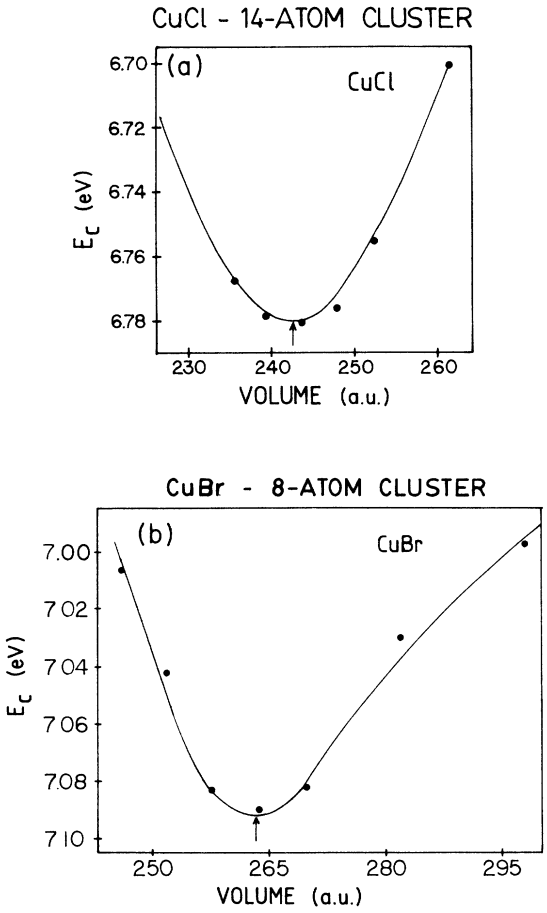

FIG. 2. (a) Cohesive energy in CuCl vs lattice volume parameter. (b) Cohesive energy in CuBr vs lattice volume parameter.

TABLE I. Structural properties of CuCl and CuBr: a is the equilibrium lattice constant in Å, E_c is the lattice cohesive energy, and B is the bulk modulus (Mbar).

Cluster description		CuCl Cu_7Cl_7	CuCl Cu_4Cl_4	CuBr Cu_4Br_4	
a (Å)	Calc.	5.24	5.38	5.39	
	Expt.[a]	5.41		5.69	
E_c (eV)	Calc.	6.78	6.62	7.09	with respect to neutral free atoms
	Expt.	5.51		5.01	
		9.62		9.37	with respect to free ions
B (Mbar)	Calc.	0.55		1.05	
	Expt.	0.38		0.39	

[a]Reference 5.

TABLE II. Equilibrium properties of CuCl and CuBr. The values in parentheses are experimental results taken from Refs. 15 and 16. All energy values are in eV.

Cluster description	Cu_7Cl_7	CuCl	Cu_4Cl_4	CuBr Cu_4Br_4
Ionicities from LS fitting	±0.43		±0.74	±0.71
Mulliken ionicities	±0.40		±0.57	±0.53
Nearest-cluster-atom-volume ionicity	±0.23		±0.47	±0.24
Band gap (eV)	1.65		1.05	0.90
		(3.3)		(~3.0)
Cu 3*d*-band center	1.70		1.40	1.5
		(1.9)		(2.05)
Halide *p*-band center	4.70		3.40	3.5
		(4.9)		(4.5)
Halide *s*-band center	15.60		14.70	13.9
		(15.8)		(15.0)
Cu 3*d*-band width	2.5		2.0	3.0
		(3.0)		(3.0)
Halide *p*-band width	3.0		3.0	4.0
		(3.0)		(3.0)

is traced to the truncation of the diffuse exchange density in the lattice sum. Such a problem is minimized in the more conventional diagonal-weighted Mulliken analysis of the charge density. For these reasons, an extended basis set, enlarged by the inclusion of unoccupied atomic orbitals, subjected to a least-squares-fitting procedure is not as good a scheme as smaller near-minimal multiple basis sets (atomic and ionic) around each atom.

From Table I, we see that the equilibrium lattice constants calculated from all three clusters are within 4% of experimental values.[14] The results for the cohesive energy for both CuCl and CuBr with respect to free neutral atoms are overestimated by about 1.27 and 2.08 eV, respectively, when compared to experiment.[15] The quality of these results is of the same order as for other solids we have studied.[12] Cohesive energies are conventionally reported in the literature with respect to free gaseous ions (9.62 eV for CuCl and 9.4 eV for CuBr); the ionization potential of Cu (7.72 eV) and the electron affinity for the halide (3.61 and 3.36 eV for Cl and Br) are invoked within the Born-Haber cycle[14] to refer the cohesion to free atoms. It is instructive to analyze the effects of our model parameters on these results. It is known that the local-density approximation is less well suited for describing the isolated atom than more extended and continuous solid systems. Also the calculated cohesive energy for CuBr exceeds that for CuCl by 0.31 eV, contrary to the experimental values, a difference which is well within the computational uncertainty.

The densities of states for CuCl and CuBr at the calculated equilibrium lattice constant are displayed in Fig. 3. The discrete energy levels have been broadened with a 0.40-eV full-width-at-half-maximum Lorentzian function to simulate solid-state bands, so band dispersions in our model are uncertain by this amount. Our results show that for both CuCl and CuBr, the uppermost valence band is narrow and mainly metal *d*-like and separated by a small gap (1.65 or 1.5 eV for CuCl from the two clusters and 0.90 eV for CuBr) from the Cu 4*s* conduction band. We observe no splitting of this *d* band into subbands. This filled d^{10} shell which participates very actively in the electronic self-consistency interactions underlies the continued interest in the cuprous halides and their fascinating properties. However, both materials are transparent which suggests that they are semiconductors with large gaps of the order of 3.3 eV for CuCl and 3.0 eV for CuBr, based on the optical (UV) absorption spectra results of Cardona.[15] The large discrepancy in our ground-state determined value for the optical gap is to be expected since the local-density approximation invariably underestimates the optical gap in semiconductors. The 0.60-eV difference in the two values of the band gap calculated for CuCl using two different clusters is partly due to the differences in equilibrium lattice constant at which they are evaluated and partly due to the very different coordination geometries within the clusters. For completeness, we mention that the calculated gap is closer in agreement to the measured activation energy [~0.39 eV (Ref. 4)], which in the context of discrete cluster eigenvalues is probably more relevant.

Below the Cu 3*d* band is a slightly broader halide *p* band, 3–4 eV wide and exhibiting very little *d*-*p* hybridization; from the area under the DOS structures, we estimate the *p*-in-*d* overlap to be ~15% in CuCl and ~25% in CuBr. About 14 eV below the Fermi energy is the halide *s* band. Except for the optical gap then, these broad features of the valence DOS, such as the ordering and placement of the valence bands are in good agreement with the photoemission data of Goldman and coworkers[16] in the UPS and XPS regimes. There the energy distribution curves (EDC) in all Cu-halide spectra are composed of two main peaks, each about 3 eV wide,

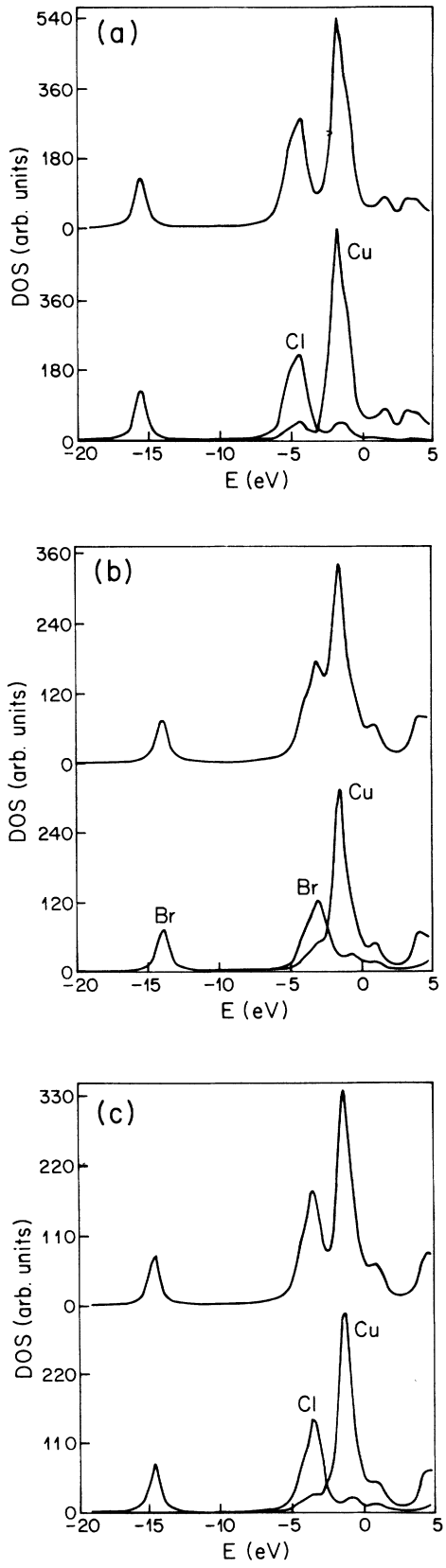

FIG. 3. (a) Total and partial DOS in CuCl from the 14-atom cluster. (b) Total and partial DOS in CuBr from the eight-atom cluster. (c) Total and partial DOS in CuCl from the eight-atom cluster.

separated by a gap which decreases as the atomic number of the halide increases. The peak in the 0–3-eV range is found to have predominantly *d*-like character; the 3–6-eV peak is recognized as the halogen *p* band; an upper limit to the *p* admixture with the upper metal *d* band is obtained as 23% for CuCl and 35% for CuBr. The 14-atom cluster gives slightly better results than the eight-atom clusters. The DOS are also in qualitative agreement with the band-structure OPW results of Overhof,[17] and the self-consistent energy band structures obtained by the *ab initio* LCAO and LMTO calculations of Freeman and co-workers.[18] Other calculated values for the optical gap in CuCl range from 0.80 eV (Ref. 18) to 3.5 eV;[17] for CuBr, Overhof obtained $E_g \sim 3.15$ eV. A MS-$X\alpha$ crystalline cluster calculation for CuCl by Guimares and Parada,[19] using five atoms to 18-atom clusters, which presages this portion of our work, accurately reproduces the band gap and is further confirmation that at least in highly ionic crystals such as CuCl cluster-size effects are not large enough to modify the qualitative behavior of the cluster energy spectrum.

B. Deformation properties

In this section we report the results of self-consistent calculations performed on CuCl and CuBr under a trigonal uniaxial strain along the [111] axis in order to determine the internal-strain parameter ζ. For the uniaxial compression in the [111] direction in the zinc-blende geometry, the [111] bond becomes inequivalent to the other bonds along the $[\bar{1}\,\bar{1}\,1]$, $[\bar{1}1\bar{1}]$, and $[1\,\bar{1}\,\bar{1}]$ directions. Consequently, the energy of the crystal can be minimized if the position of the second atom in the primitive cell shifts not just with the homogeneous deformation but rather relaxes in accordance with the internal strains. For an applied stress along the [111] axis, the volume-conserving trigonal uniaxial macroscopic strain tensor can be written as[20,21]

$$\vec{\epsilon}=\epsilon\begin{bmatrix}0&1&1\\1&0&1\\1&1&0\end{bmatrix}. \tag{13}$$

The effects of this strain on the vectors from a central atom to its four tetrahedrally coordinated neighbors is given by

$$\begin{aligned}
\mathbf{r}_1&=\frac{a_0}{4}(1,1,1)\rightarrow\frac{a_0}{4}(1+2\sigma,1+2\sigma,1+2\sigma)\,,\\
\mathbf{r}_2&=\frac{a_0}{4}(-1,-1,-1)\\
&\rightarrow\frac{a_0}{4}(-1-2\epsilon\zeta,-1-2\epsilon\zeta,1-2\epsilon-2\epsilon\zeta)\,,\\
\mathbf{r}_3&=\frac{a_0}{4}(1,-1,-1)\\
&\rightarrow\frac{a_0}{4}(1-2\epsilon-2\epsilon\zeta,-1-2\epsilon\zeta,-1-2\epsilon\zeta)\,,\\
\mathbf{r}_4&=\frac{a_0}{4}(-1,1,-1)\\
&\rightarrow\frac{a_0}{4}(-1-2\epsilon\zeta,1-2\epsilon\zeta,-1-2\epsilon\zeta)\,,
\end{aligned} \tag{14}$$

where $\sigma=\epsilon(1-\zeta)$.

For the above geometry we have calculated the changes in lattice energy as a function of the [111] Cu-halide bond length (equal to b) on applying a strain $\epsilon\sim 2.125\%$. The calculated values closest to the minimum are then fitted to a second-order polynomial. The clusters employed are Cu_7Cl_7 and Cu_4Br_4, respectively, with results shown in Fig. 4 along with the change in ionicity for the Cu atom. For CuCl the energy minimum occurs at $b=4.34$ a.u. which corresponds to $\zeta=1.26$. It implies that a small uniaxial compression along [111] results in the Cu—Cl bond elongating beyond its equilibrium length by 0.05 a.u.; this is clearly an untenable result. This is partly the consequence of using a football-shaped cluster. To investigate this cluster-shape effect we relaxed the sublattice position in the unstrained lattice from its idealized experimental position at $\frac{1}{4}$ along the calculated equilibrium body diagonal (4.29 a.u.). When b is expanded from 4.29 a.u. to 4.32, 4.35, and 4.38 a.u., the cohesive energy increases by 0.0022, 0.0028, and 0.0006 eV, respectively; the minimum corresponds to a bond length $b=4.332$ a.u. If ζ is now interpreted as the internal relaxation in the (111) cluster bond length and calculated with reference to $b=4.332$ a.u., our new value of ζ is 1.05. Within the limits of computational precision which can be enhanced by choosing a larger value for the macroscopic strain ϵ, say $\epsilon\sim 4.0\%$, this value indicates a very rigid Cu—Cl bond. In view of this small softening effect, there is no need to remap the a-b potential surface. For CuBr the energy minimum occurs for $b=4.40$ a.u. which translates into $\zeta=0.94$. For the unstrained lattice, two self-consistent calculations with the bond length b expanded and contracted from its ideal length 4.41 by 0.03 a.u. show that for this cluster the [111] bond length is 4.41 a.u. Considering again the dispersion of the calculated energy values we translate the limited resolution of the exact position of the curve minima into error bars on the values of ζ: ± 0.15 for CuCl and ± 0.10 for CuBr.

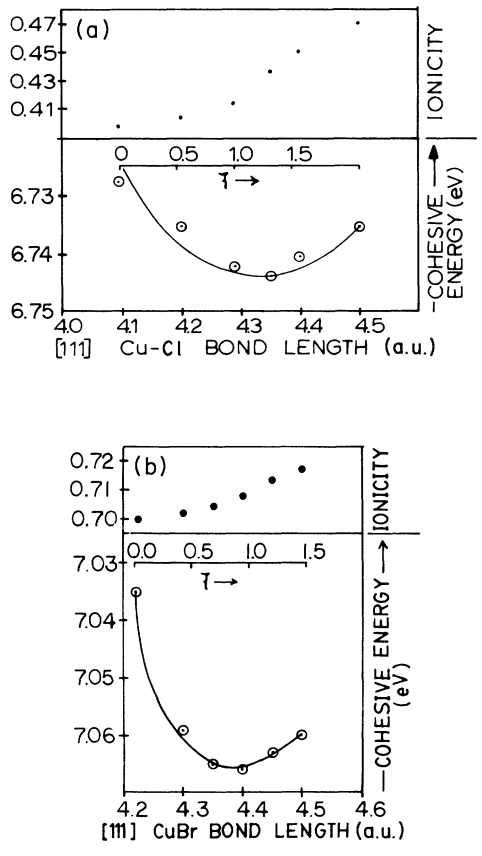

FIG. 4. (a) Internal strain parameter ζ and change in ionicity in CuCl as a function of the Cu—Cl bond length under uniaxial [111] strain. (b) Internal strain parameter ζ and change in ionicity in CuBr as a function of the Cu—Br bond length under uniaxial [111] strain.

Experimental determinations of ζ are based on the measurement of the increase in intensity for forbidden x-ray reflections upon application of uniaxial stress along [111]. In zinc-blende structures, these forbidden reflections are lifted due to the difference in atomic form factors of the two atoms in the primitive cell so that one has to rely upon theoretical values of ζ. From a simple valence-forcefield approach, which utilizes bond-stretching (α) and bond-bending (β) forces coupled with effective point-ion Coulomb forces, Martin[2] has derived a value $\zeta=0.87$ for CuCl and $\zeta=0.85$ for CuBr. More recently, Christensen[22] has calculated the deformation potentials for uniaxial-strain-induced splitting in the top of the valence bands as a function of the uniaxial strain parameter ζ for the cuprous halides. Although the scatter in the experimental data is too large to allow an accurate determination of ζ, Christensen concludes that $\zeta\sim 1$ or perhaps larger than 1 for both CuCl and CuI. These are the only two direct calculations of ζ in CuCl that we are aware of. Our results for CuCl are in agreement with the above though it cannot be said that they determine ζ to any greater precision.

C. Piezoelectric parameters

Following the prescription of Martin and Kunc,[8] we have computed the longitudinal and transverse effective charges and quadrupole moments for both CuCl and CuBr. The clusters employed for these calculations are Cu_4Cl_4 and Cu_4Br_4. In these calculations the restraint of full periodicity is removed, each layer of atoms along [111] being allowed independent variation. For each solid, two independent self-consistent calculations of the electronic charge density are made, first with the layer of the single Cu_1 atom displaced by $+0.05$ a.u. along [111] and then with the layer of the single halide atom displaced by -0.05 a.u. along [111]. This displacement pattern is repeated in every third layer pair along [111], ~ 17.65 a.u. apart. It is assumed that this repeat distance is large enough that the potential and charge density have converged to their bulk values in the intermediate regions. In addition a 0.05 a.u. displacement is assumed to produce linear change in the charge density. Since these small clusters contain only two layer pairs of the 012012... stacking, we have had to make approximations in the two layer pairs in which there are no atom displacements by treating them on an equal footing.

In the actual calculation, once the self-consistent

charge densities for the crystal with a single plane of displaced atoms is required, e_L and Q_L are obtained by computing the numerical difference derivatives of the charge density on a fixed grid of sampling points, that does not move with the displaced atoms. For a small displacement 0.05 a.u. the error introduced thereby is insignificant. We then use the known values of the static dielectric constant $\epsilon_s = 7.0$ for CuCl and $\epsilon_s = 6.6$ for CuBr to obtain e_T and ΔQ from Eqs. (7) and (8). These results are presented in Table III.

There have been several calculations of the macroscopic effective charge in the literature.[23–25] The magnitude of e_T can be obtained experimentally from the difference between the squares of the long-wavelength LO- and TO-mode frequencies

$$\omega_L^2 = \omega_T^2 + \frac{4\pi e_T^2}{\epsilon_\infty \overline{m} V_0} , \tag{15}$$

where $\overline{m}$ is the reduced mass of the atoms in the primitive cell, V_0 is the volume of a primitive cell, and ϵ_s and ϵ_∞ are the static and high-frequency dielectric constants. Using $\omega_L = 196$ cm^{-1}, $\omega_T = 141$ cm^{-1} (Ref. 26), and $\epsilon = 3.61$ we obtain $e_T = 1.11e$ for CuCl. With $\omega_L = 165$ cm^{-1}, $\omega_T = 125$ cm^{-1}, and $\epsilon = 3.71$ for CuBr gives $e_T = 1.16e$.

In crystals which are predominantly ionic, the values of these dynamic effective charges do not in general differ appreciably from the static ionic charges, i.e., $e_T f_i$, where f_i is the spectroscopic ionicity of Phillips and Van Vechten.[1] However, in zinc-blende-type crystals for which covalent contributions are equally as or more important than the ionic contributions, e_T is of the order of 2.0. Lucovsky and co-workers[25] derive a value $e_T = 1.12$ for CuCl by decomposing the TO-phonon frequency into two components, one associated with short-range forces giving a localized effective charge e_1, and the other e_T associated with the dipolar interactions. The I-VI crystals are found to have anomalously low values of e_T which, unlike for the other zinc-blende structures, do not scale with the Phillips ionicity.

We estimate e_T/e for CuCl and CuBr to be 1.30 and 1.40, respectively, from our self-consistent calculations of change in the charge density induced from a small displacement of a single atomic plane along (111). The integration errors are satisfyingly small so that the neutrality condition is seen to be preserved within the computational precision. Our values for e_T are slightly higher than the experimental results by about 0.2 and 0.25, respectively: it is worthwhile to investigate the sources of this discrepancy since they are applicable to the discussion of the quadrupole moments also. If the superlattice constant along the (111) axis, a $\sqrt{3}$, is not large enough to make the displacements of the atomic planes independent of each other, in the true spirit of a supercell calculation, then the more diffuse Br orbitals would cause the relative integration errors due to truncation of our integrals to exceed the error in the CuCl calculation. We see, however, that the spread in e_L/e for CuBr is only in excess of that for CuCl by 0.003, an indication that the overlap across the supercell boundary is small. The dominant factor influencing our results is that the process of averaging the atomic configurations over the two layer pairs that are not subject to an atomic-plane displacement in effect drives the charge density in the displaced atomic-plane system more slowly from the equilibrium charge density than if both these layer pairs were allowed independent variation. This particular consequence is a

TABLE III. Results for the cluster calculations on CuCl and CuBr under a (111) strain, $\epsilon \sim 2.1\%$. The atomic orbital populations are calculated using the value of ζ closest to the energy-minimized value.

Cluster description		CuCl Cu_7Cl_7	CuCl Cu_4Cl_4		CuBr Cu_4Br_4
Orbital	Cu 3*s*	2.066	2.032		2.046
populations	3*p*	5.966	6.008		6.005
(from LS fitting)	3*d*	9.840	9.815		9.705
	4*s*	0.239	0.641		0.830
	4*p*	0.414	−0.073		−0.094
	5*s*	−0.511	−0.441		−0.585
	5*p*	0.549	0.286		0.425
	Cl 3*s*	1.649	1.595	Br 4*s*	1.897
	3*p*	5.366	5.319	4*p*	4.737
	3*d*	0.419	0.633	4*d*	0.976
	4*s*	0.740	0.892	5*s*	−0.008
	4*p*	−0.737	−0.707	5*p*	0.066
Ionicities		±0.437	±0.732		±0.668
ζ		1.25	1.05±0.15		0.94±0.10
e_L(Cu)/*e*		0.224	0.180		0.209
e_L(halide)			−0.188		−0.220
e_T(Cu)/*e*		1.57	1.26		1.38
e_T(halide)/*e*			−1.32		−1.45
$\frac{a^2 Q_L}{eV_0}$			0.006		0.014

function of the atom coordination within the cluster and there is no *a priori* way of determining the direction of its effects. Secondly, the least-squares fitting of the cluster charge density, which enables us to project the latter onto superposed spherical atomic configurations, is not perfectly capable of tracking the charge redistribution due to the displaced plane of atoms. Both these approximations, in fact, serve to underestimate the induced charge density and to bring e_T closer to the experimental result.

Quadrupole moments of the induced charge density are a measure of the charge-response delocalization and are important in understanding the interatomic forces in ZnS and diamond-structure crystals.[27] Lawaetz[23] has argued from an empirical analysis of the piezoelectric constant e_{14} for a considerable number of materials having ZnS or wurtzite structure that the quadrupole ΔQ and dipole e_T contributions in Eq. (12b) are related by $\Delta Q = 0.75 e_T$, a seemingly intrinsic property of the fourfold coordination. The scaled dimensionless quadrupole moments of the induced charge density due to a single plane of displaced atoms calculated in this work are distinguished by their small values, 0.006 and 0.014 for CuCl and CuBr, respectively. The analysis of errors and approximations discussed above for e_T are applicable here too. The main contributions to the integrals for Q_L, using the model charge density, comes from the charge-transfer term between the atomic layers, i.e., due to changes in the static least-squares ionicities. Since changes in the ionicities are inhibited by the averaging process discussed above, we may conclude that our values for Q_L and Q_T are underestimates of the actual quadrupole moments in the cuprous halides. Even so, our results appear to suggest that the quadrupoles decrease rapidly relative to the dipoles with increasing ionicity as the rigid-ion behavior is approached. From Eq. (12b) for the piezoelectric constant e_{14}, it is easy to see why the cuprous halides have the largest piezoelectric constants among the zinc-blende structures: charge redistribution due to internal strain wholly dominates over the charge-transfer quadrupolar contribution. Using Hanson's experimental values for e_T and our calculated values for ζ in Eq. (12b), we obtain $\Delta Q = 0.54$ for CuCl and 0.55 for CuBr. The relative magnitudes of Q_L determined here are even further apart than these results.

Since the input specifications for cluster calculations on both CuCl and CuBr are identical, our results for e_T and Q do bear comparison in a relative sense. Thus in an AB compound, both e_T and Q increase as, with A fixed, B is lower down in a column of the Periodic Table. The sharp decrease in Q by a factor of more than 2 in going from CuBr to CuCl corresponding to a comparatively small increase in the spectroscopic ionicities from 0.735 to 0.746 is symptomatic of the anomalous rigid-ion behavior that is at the source of the structural instability in zinc-blende structures near the critical ionicity $f_1 = 0.785$.

V. CONCLUSION

In summary, self-consistent calculations of equilibrium and deformation properties of the cuprous halides, CuCl and CuBr, have been carried out using embedded clusters within an LCAO-MO approach. We find that moderately large atomic basis sets on each atom species in reasonably small clusters oriented along [111] yield equilibrium lattice constants within 4% of the experimental value and cohesive energies with respect to free neutral atoms which are overestimates of the bulk values by 1.25–2.1 eV. The band structure from the cluster levels shows a filled $3d^{10}$ band at the Fermi energy and is in good agreement with experiment and band features from other models. Under a [111] compression of 2.1%, the internal relative relaxation of the halide sublattice is such that the Cu-halide bond remains rigid and unstretched after cluster shape and size effects have been accounted for, the internal strain parameters are determined to be 1.05 and 0.94, respectively, for CuCl and CuBr, in agreement with previous estimates. Finally, the transverse effective charge e_T, computed as the first moment of the induced charge density following the displacement of a (111) atomic plane by 0.05 a.u. along [111], is estimated to be 1.30 for CuCl and 1.40 for CuBr. The quadrupole moment contributions, i.e., the second moment of the induced charge density are remarkably small, an indication of very little charge transfer between the rigid-ion layers and symptomatic of the anomalous behavior of the zinc-blende structure near the critical ionicity.

ACKNOWLEDGMENTS

This work was supported by the National Science Foundation through the Materials Research Center of Northwestern University (Grant No. DMR 85-20280).

[1] J. C. Phillips and J. A. Van Vechten, Phys. Rev. Lett. **23**, 1115 (1969).

[2] R. M. Martin, Phys. Rev. B **1**, 4005 (1970).

[3] R. C. Hanson, J. R. Halberg, and C. Schwab, Appl. Phys. Lett. **22**, 490 (1972).

[4] A. P. Rusakov, Phys. Status Solidi B **72**, 503 (1975); C. W. Chu, A. P. Rusakov, S. Hwang, S. Early, T. H. Geballe, and C. Y. Haung, Phys. Rev. B **18**, 2116 (1978).

[5] H. K. Wong, G. K. Wong, and J. B. Ketterson, J. Appl. Phys. **53**, 6834 (1982).

[6] For classic references on the classical theory of piezoelectricity: M. Born and K. Hwang, *Dynamical Theory of Crystal Lattices* (Oxford University Press, England, 1954), Chap. 5; W. F. Cady, *Piezoelectricity* (McGraw-Hill, New York, 1946); J. F. Nye, *Physical Properties of Crystals* (Oxford University Press, England, 1957), Chap. 10.

[7] R. M. Martin, Phys. Rev. B **5**, 1607 (1972).

[8] R. M. Martin and K. Kunc, Phys. Rev. B **24**, 2081 (1981); K. Kunc and R. M. Martin, *ibid.* **24**, 2311 (1981).

[9] G. Arlt and P. Quadflieg, Phys. Status Solidi **25**, 323 (1968); R.

M. Martin, Phys. Rev. B **6**, 4546 (1972).
[10]L. Kleinman, Phys. Rev. **128**, 2614 (1962).
[11]D. E. Ellis and G. S. Painter, Phys. Rev. B **2**, 2887 (1970); E. J. Baerends, D. E. Ellis, and P. Ros, Chem. Phys. **2**, 41 (1973); D. E. Ellis, G. A. Benesh, and E. Byrom, Phys. Rev. B **16**, 3308 (1977); B. Delley and D. E. Ellis, J. Chem. Phys. **76**, (4), 1949 (1982).
[12]M. R. Press, Ph.D thesis, Northwestern University, Evanston, IL, 1986.
[13]M. R. Press and D. E. Ellis, Phys. Rev. B **35**, 4438 (1987); P. K. Khowash and D. E. Ellis, *ibid.* **36**, 3396 (1987).
[14]M. P. Tosi, in *Solid State Physics,* edited by F. Seitz and E. Turnbull (Academic, New York, 1964), Vol. 16, p. 1.
[15]M. Cardona, Phys. Rev. **129**, 69 (1963).
[16]A. Goldman, J. Tejeda, N. J. Shevchik, and M. Cardona, Phys. Rev. B **10**, 4388 (1974).
[17]H. Overhof, Phys. Status Solidi B **97**, 267 (1980).
[18]A. J. Freeman, C. S. Wang, T. Jarlborg, M. Weinert, F. Wagner, and C. W. Chu, Int. J. Quantum Chem. **13**, 445 (1979).
[19]P. S. Guimares and N. J. Parada, J. Phys. C **17**, 1695 (1984).
[20]J. L. Birman, Phys. Rev. **111**, 1510 (1958).
[21]F. Cerdeira, C. J. Buchenauer, F. H. Pollak, and M. Cardona, Phys. Rev. B **5**, 580 (1972).
[22]N. E. Christensen, Phys. Status Solidi B **123**, 281 (1984).
[23]P. Lawaetz, Phys. Status Solidi B **63**, 485 (1974).
[24]E. Burstein, M. H. Brodsky, and G. Lucovsky, Int. J. Quantum Chem. **1s**, 759 (1967).
[25]G. Lucovsky, R. M. Martin, and E. Burstein, Phys. Rev. B **4**, 1367 (1971).
[26]I. P. Kaminov and E. H. Turner, Phys. Rev. B **5**, 1564 (1972).
[27]M. Lax, in *Lattice Dynamics,* edited by R. Wallis (Pergamon, Oxford, 1964), p. 179.